Organic & Biomolecular Chemistry

Cite this: *Org. Biomol. Chem.*, 2012, **10**, 6287

www.rsc.org/obc

PAPER

From pico to nano: biofunctionalization of cube-octameric silsesquioxanes by peptides and miniproteins†

Sebastian Fabritz,‡[a] Sebastian Hörner,‡[a] Doreen Könning,[a] Martin Empting,[a] Michael Reinwarth,[a] Christian Dietz,[b] Bernhard Glotzbach,[a] Holm Frauendorf,[c] Harald Kolmar*[a] and Olga Avrutina*[a]

Received 13th April 2012, Accepted 11th June 2012
DOI: 10.1039/c2ob25728a

Polyhedral silsesquioxanes are considered valuable conjugation scaffolds. Nevertheless, only a few examples of silsesquioxane-assembled peptide oligomers have been reported to date. We developed a new bioorthogonal cube-octameric silsesquioxane (COSS) scaffold bearing eight aminooxy coupling sites allowing for the conjugation of diverse peptides *via* oxime ligation. We found that the coupling efficacy depends on the ligand in view of steric hindrance and electrostatic repulsion. For the first time scaffold-based conjugation of cystine-knot miniproteins having a backbone of about thirty amino acids was successfully accomplished without loss of bioactivity. Atomic force microscopy (AFM) provided further knowledge on the size of COSS verifying them as picoscaffolds growing upon bioconjugation to nano-dimension.

Introduction

Combining several ligands on a single scaffold often results in improved characteristics of a formed oligomer compared to its individual constituents. Nature extensively uses this phenomenon known as multivalency to effect biomolecular interactions[1] in living organisms by enhancing affinity and specificity of binding.[2] This inspires research efforts towards creation of synthetic molecules in which the benefits of simultaneous multiple contacts are achieved through the oligomerization of bioactive modules – small molecules,[3] carbohydrates,[4] peptides,[5] and proteins.[1] Properties of scaffold-grafted molecular blocks are often governed by the peculiar architecture that implies shape, size, and valency of the framework, as well as spatial orientation of ligands.[6]

In recent years, cube-octameric silsesquioxanes (COSS)[7,8] have been brought into focus as promising oligomerization scaffolds due to their unique characteristics. These monodisperse particles with a core size of 0.5 nm[9] are considered the smallest known nanoscaffolds with a high degree of symmetry. Their hybrid molecules are composed of a siloxane inorganic core decorated with organic ligands which combine an aliphatic linker with a terminal active group. From a broad repertoire of functionalized COSS molecules reported to date, amine,[10] azide,[11–13] alkyne,[12] thiol,[14] aldehyde[15] or maleimide bearing[16] particles are potentially applicable for bioconjugations.

To date, several COSS-based bioconjugates have been reported, among them lysine dendrimers for drug delivery,[17,18] oligomers of peptides[12,19] and carbohydrates,[13,20] as well as macrocyclic Gd^{3+} chelates as potential magnetic resonance imaging contrast agents.[21]

The convergent synthesis of peptidic COSS is limited to homopolypeptides where one amino acid unit with a protected or non-reactive side chain is propagated,[22,23] or to rather short (up to 8 residues) RGD oligomers.[12] In these bioconjugations, copper-catalyzed azide–alkyne cycloaddition (CuAAC) is currently the established method to obtain a linkage between an azide-bearing silsesquioxane and an alkyne-modified peptidic ligand usually added in stoichiometric excess.[24,25] Due to the instability of a COSS core in the presence of aqueous nucleophiles,[21,26] CuAAC with silsesquioxanes is generally performed in water-free DMF.[12,27,28] In this aprotic solvent, the copper catalyst often appeared to be coordinated by an amide backbone[29] or functional side chains[30] of peptides leading to a drastic decrease of active catalytic species and, as a consequence, to prolonged reaction times (up to several weeks) and low yields.[12] Very recently, an elegant alternative approach to silsesquioxane-based peptide conjugations has been reported which utilized the photo-induced free-radical thiol–ene coupling and resulted in eightfold presentation of the tripeptide glutathione on a COSS scaffold.[31,32] Interestingly, for a tetrapeptide RGDC complete

[a]*Clemens-Schöpf Institute of Organic Chemistry and Biochemistry, Technische Universität Darmstadt, Petersenstr. 22, 64287 Darmstadt, Germany.*
E-mail: Kolmar@Biochemie-TUD.de; Avrutina@Biochemie-TUD.de
[b]*Center of Smart Interfaces, Technische Universität Darmstadt, Petersenstr. 32, 64287 Darmstadt, Germany*
[c]*Institute of Organic and Biomolecular Chemistry, Georg-August Universität Göttingen, Tamannstraße 2, 37077 Göttingen, Germany*

†Electronic supplementary information (ESI) available: ^{1}H-NMR and ^{29}Si-NMR data of **2**, **3**; ESI-MS data of **2–9**; IR spectra of **2**, **3**. See DOI: 10.1039/c2ob25728a

‡These authors contributed equally to this work.

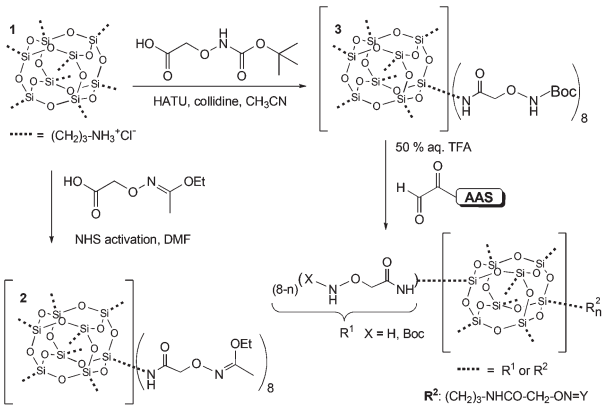

Peptidic Ligands

Amino Acid Sequence (AAS)	Precursor	Conjugate	
	HO, H_2N, HN—AAS	Y= AAS, O	n
IPRGDYRKG-OH	**p4**	**4**	8
LHLSLKFPG-OH	**p5**	**5**	8
INLKALAALAKKINL-NH_2	**p6**	**6**	6
GVCPKILKKCRRDSDCPGACICRGNGYCG-NH_2	**p7**	**7**	3
WGVCPKVLRNCRRDSDCPGACICLGNGYCG-NH_2	**p8**	**8**	3
$(KVSALKE)_5$-NH_2	**p9**	**9**	2

Scheme 1 Synthetic approaches to protected aminooxy COSS **2** and **3**. Octakis (Boc-aminooxy) COSS was used as a scaffold for bioconjugation. Ligands: an octapeptide with an RGD motif (**p4**), a derivative of the antimicrobial peptide Jelleine 1 (**p5**), mastoparan (**p6**), MCoTI-based miniproteins (**p7**, **p8**) and Kcoil, a basic α-helical coil (**p9**), were chosen.

hydrothiolation of vinyl coupling sites was achieved only after the introduction of elongation linkers.[31]

Herein, we report bioconjugation on a COSS scaffold in acidic aqueous media based on the oxime ligation[33,34] between an aldehyde and an aminooxy functionality (Scheme 1). This approach provides several advantages compared to other methods reported for COSS–peptide conjugations[12,27,28,31,32] as it ensures both stability of the silsesquioxane core and good solubility of biological ligands. The introduction of aldehyde moieties into biomolecules is well-established and can easily be achieved *via* periodate oxidation of an N-terminal serine residue.[35] Moreover, building blocks for solid phase peptide synthesis[36,37] containing a masked side-chain aldehyde function enable the generation of this moiety at any desired sequence position. Aminooxy functionality can be easily introduced in peptides by N-acylation of side-chain or terminal amines by butoxycarbonyl (Boc)[38] or ethoxyethylidene (Eei)[39,40] protected aminooxy acetic acid. Protection is essential to avoid side reactions and overacylation of target compounds. In the present research, the applicability of the oxime ligation to the synthesis of hybrid COSS–peptide conjugates was studied highlighting the benefits and the limitations of the method.

Results and discussion

As a conjugation scaffold an octaaminopropyl-COSS **1** was used. The reaction with commercially available mono-Boc aminooxy acetic acid towards **3** appeared strongly dependent on the activation conditions leading to overacylated species (Table 1).

Decostaire *et al*. have recently reported[38] that the control over these undesired processes could be achieved by the proper choice of used activator, base, and solvent as well as their excess. Corroborating the reported data,[38] 2-(7-aza-1*H*-benzotriazole-1-yl)-1,1,3,3-tetramethyluronium hexa-fluoro-phosphate (HATU) activation in the presence of collidine was found to be the optimal reaction conditions, and 20 equivalents of the base per silsesquioxane octamer were used (Fig. 1). Although no overacylated COSS species have been found in both acetonitrile- and DMF-based reaction mixtures (Table 1, entries 5 and 6), dry acetonitrile appeared to be the solvent of choice as no complete

Table 1 Reaction conditions for the synthesis of **3**

No.	Solvent	Base equiv. (collidine)	Activator (8 × 5.2 equiv.)	Overacylated 0	×1	×2	×3
1	DMF	85	HBTU	X	X	X	X
2	DMF	43	HBTU	X	X	nd	nd
3	DMF	53	HATU	X	X	nd	nd
4	MeCN	53	HATU	X	X	X	X
5	MeCN	20	HATU	X	nd	nd	nd
6	DMF	20	HATU	X[a]	nd	nd	nd

X: detected; nd: not detected.[a] Reaction showed incomplete conversion. Heptameric Boc-aminooxy COSS species were detected *via* LC-MS analysis.

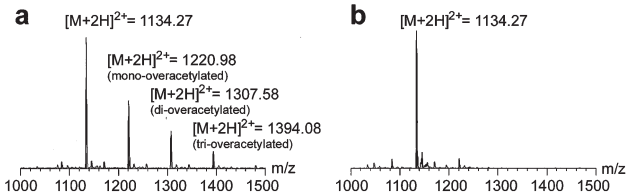

Fig. 1 ESI-MS spectra for the synthesis of **3**. (a) Reaction in DMF using HBTU and 85 equiv. collidine; (b) reaction in MeCN using HATU and 20 equiv. collidine.

conversion was observed in DMF after an overnight reaction. Contrary to this procedure, reaction of **1** with *N*-hydroxysuccinimide-activated 2-(1-ethoxy-ethylidene-aminooxy) acetic acid[40] resulted in octakis Eei-protected aminooxy-COSS **2** without overacylation. Due to the instability of COSS in the presence of aqueous nucleophiles,[21,26] the cage integrity of **2** and **3** was verified by ^{29}Si-NMR and IR spectroscopy (see ESI Fig. S3, S4 and S6†). The NMR spectra showed exclusively the shifts corresponding to COSS cages **2** and **3** (δ −66.87 and δ −66.75, respectively). The IR spectra showed a Si–O–Si stretch characteristic band at 1115 cm^{-1}. Both Boc and Eei groups were cleaved in 50% aqueous trifluoroacetic acid (TFA) within 3 hours, and one-pot conjugation with aldehyde functionalized peptides[35] succeeded. In our study, ligands with diverse primary

and secondary structures and different bioactivity were used (Scheme 1).

For the initial experiment, an integrin-binding octapeptide bearing an RGD functional motif (**p4**) was chosen.[41,42] It was shown previously that this ligand could be coupled onto the COSS scaffold in eightfold copies *via* CuAAC.[12] We found that oxime ligation had obvious benefits compared to CuAAC as the reaction time needed for full conversion was drastically reduced – from several weeks to an overnight reaction at room temperature. LC-MS monitoring of the reaction progress showed the presence of COSS species bearing both protected aminooxy coupling sites and oxime-ligated peptides (see ESI Fig. S8†), indicating that Boc cleavage was the rate-determining step. Nevertheless, as soon as full deprotection was achieved, the steric hindrance and electrostatic repulsion caused by the growing number of peptidic ligands seemed to have a major influence on the reaction progress.

Consequently, we explored the ligand-dependent limitations of the proposed COSS-based oximation. It is obvious that direct coupling of bulky peptide ligands onto constrained COSS scaffolds can be hindered due to steric reasons. On the other hand, often the oligomerization of peptides and full-size proteins is desirable without implementation of elongation linkers. Therefore, in a series of coupling experiments the size of bioactive peptidic ligands was progressively increased from eight (**p4**) to 35 (**p9**) amino acid residues.

To that end, a derivative of natural antimicrobial peptide Jelleine 1[43,44] from the royal jelly of honey bees (**p5**) was used. The successful eightfold presentation of this octapeptide on the COSS scaffold encouraged us to approach more sophisticated ligands. Thus, an α-helical calmodulin[45] binding peptide mastoparan (**p6**)[46] comprising 14 residues, trypsin inhibitors[47] **p7** and **p8** having 29 and 30 residues, respectively, and the inherent Kcoil part of a heterodimeric coiled coil (**p9**)[48–50] with a length of 35 amino acids were used. Moreover, miniproteins[51] **p7** and **p8** contained a characteristic tri-disulfide pattern known as a cystine knot[52] that is absolutely essential for the function; the damage of this motif results in the loss of three-dimensional structure and, as a consequence, of bioactivity.[52]

All peptidic ligands contained, compared to their parent sequences, an additional N-terminal serine and were assembled by standard microwave-assisted Fmoc-SPPS as previously described.[53] After chain assembling and cleavage from the support, sodium periodate oxidation resulted in peptide aldehydes.[35] In the case of miniproteins **p7** and **p8**, oxidative folding[54] into a cystine knot preceded the formation of an N-terminal glyoxal.

One-step deprotection of **3** followed by conjugation with peptidic ligands **p5–p9** was performed in 50% aqueous TFA as described above. The LC-MS monitoring of the conjugation reaction with cystine-free ligands revealed the formation of COSS–peptide intermediates after 10 min. Within 12 hours the reactions were completed. The formation of miniprotein–COSS conjugates **7** and **8** was only observed after an overnight reaction. This might be attributed to a hindered accessibility of the miniprotein aldehyde functionalities.

The amount of ligand copies attached to the COSS core correlated with the primary structure of the peptides and the increasing steric demand. Thus, the conjugation with the Jelleine-derived octapeptide **p5** yielded an octameric product. Mastoparan **p6** with just 6 additional amino acids formed a hexameric conjugate. In miniproteins **p7** and **p8** the amount of amino acids is doubled compared to **p6** resulting in a decreased coupling efficacy. Accordingly, only di- as well as trimeric constructs were observed for these ligands (Fig. 2). Finally, the pronounced steric hindrance as well as the possibility of strong electrostatic

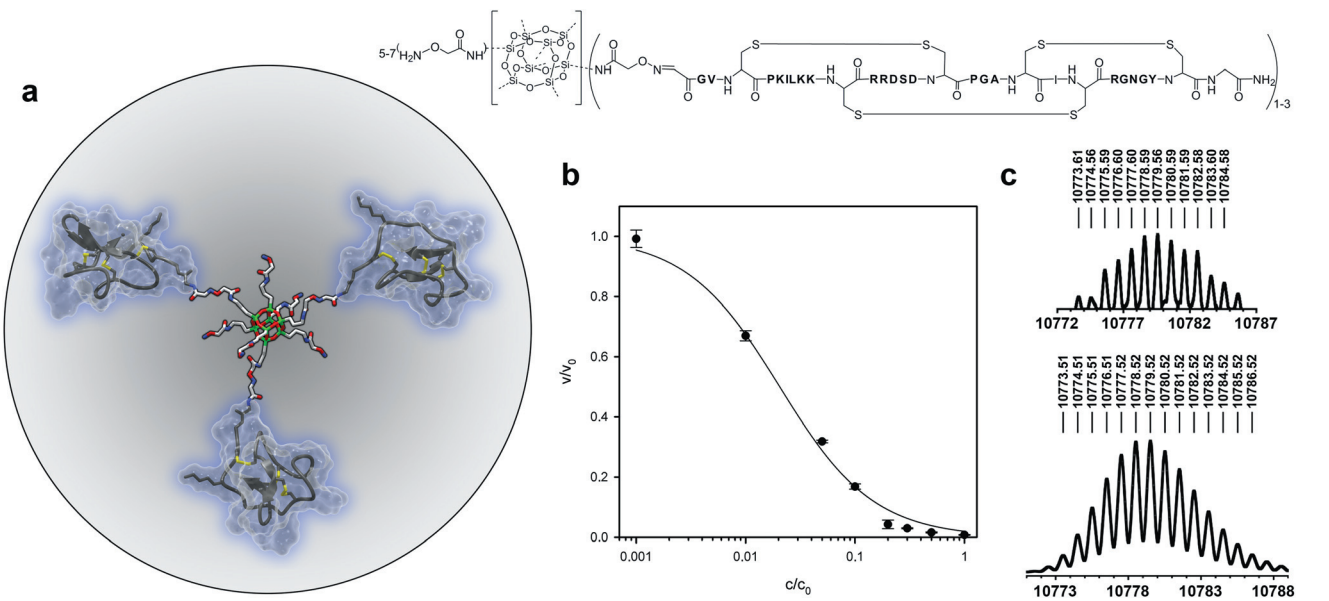

Fig. 2 (a) Proposed YASARA model of a miniprotein–COSS conjugate (pale blue: MCoTI miniproteins with disulfide bridges depicted as yellow sticks; red: oxygen; blue: nitrogen; green: silicon; grey: carbon) and its chemical structure. (b) Inhibition of trypsin-catalyzed proteolysis of chromogenic substrate *Boc*-QAR-*pNA* by conjugate **7**. Trypsin fractional activity is plotted as a function of inhibitor concentration on a log scale.[56] (c) Observed (top) and simulated (bottom) HR-MS spectra of **7**.

repulsion allowed only for the formation of mono- and dimeric products with the α-helical Kcoil peptide **p9**.

To the best of our knowledge, to date the dimerization of miniproteins was only facilitated *via* chemical cross-linking using a bis-succinimidyl suberate.[55] Herein, we present the first scaffold-based approach to the oligomerization of miniproteins. To examine whether cystine knot protease inhibitors retained their unique three-dimensional structure after conjugation, we studied the bioactivity of formed hybrid molecules. To that end, an RP-HPLC fraction containing conjugate **7** and lower substituted COSS–**p7** conjugates was tested for inhibitory activity against trypsin (Fig. 2).[56] Although a precise determination of inhibitor concentrations in the mixture of tri-, bi- and monoconjugated miniproteins was not possible and corresponding inhibition constants were not calculated, the concentration-dependent inhibition of trypsin-mediated proteolysis provided clear evidence that the bioactivity of **p7** was preserved under oximation conditions.

The bioactivity and toxicity of nanoparticles as well as their potential for drug delivery is greatly dependent on the size. Therefore, we conducted atomic force microscopy (AFM) experiments using the particles **1**, **4**, and **5**. We considered mica (negatively charged sheet silica) an optimal substrate, as the eight amino groups of **1** and the peptidic side chains of **4** and **5** promised a good binding to this surface. The dropcasting of an acidic solution of **1** (~1 ng mL^{-1}) allowed us to visualize singular particles. The enumeration of 60 particles (see ESI Fig. S7† and Fig. 3d) resulted in an average particle size of 743 ± 211 pm. This value is in good accordance with the literature stating ~500 pm for the POSS core.[8,9] For further measurements a mica substrate was dipcoated with an RP-HPLC fraction containing **4**. An analysis of the particle size distribution revealed an average size of 1810 ± 300 pm. Hence, the peptidic shell induced a measurable size increase of 1050 pm. On a first glance, this value seemed to be rather small compared to a rough simulation of **4** predicting 6.42 ± 0.69 nm as its maximal diameter in solution (see ESI Fig. S12†). However, it has to be taken into account that the particle is absorbed on a mica surface and might adopt a pancake-like structure. Furthermore, the recorded topography of a sample always depends on several parameters. Being operated in tapping mode, the AFM *z*-piezo detects changes upon the interaction of its tip with an analyzed sample keeping the amplitude of the vibrating cantilever constant. If attractive van der Waals forces change due to differences in the Hamaker constant[57] between two materials, the *z*-piezo will compensate this difference by varying the mean distance between the tip and the sample. On soft materials, compared to the sample substrate, an additional difference of the indentation depth of the tip into the material is compensated by the *z*-piezo. As a consequence, even for atomically flat surfaces a non-negligible height profile can be measured for inhomogeneous samples.[58] Hence, the measured height differences should only be used to classify the nanoparticle dimension.

The subsequent analysis of **5** revealed, in accordance with the expectations, particles with a similar height profile. Therefore, we chose a random particle and continuously increased its mapping resolution using bimodal atomic force microscopy. Fig. 4a shows the high resolution phase image of the second eigenmode. Phase images in AFM are related to mechanical properties of the sample. Three regions with a distinctive phase shift between cantilever oscillation and excitation were identified. The difference in phase values of mica ($\Delta\varphi_2$ = 120°) and the main body of the particle ($\Delta\varphi_2$ = 119°) can be attributed to the mechanical dissimilarity of the materials. A region with a relatively low phase shift ($\Delta\varphi_2$ = 110°) was found in the right part of the particle (Fig. 4b). An image artefact can be excluded since the same area was successively scanned several times depicting comparable contrast. We presume that this region might visualize the position of the mica-adsorbed silsesquioxane core surrounded by randomly oriented peptide chains (Fig. 4d).

Conclusion

A new bioorthogonal COSS scaffold was developed comprising a highly symmetric silsesquioxane core decorated with aminooxy functional modules. We demonstrated the applicability of this scaffold for the oligomerization of aldehyde-bearing peptidic ligands through oxime ligation. Our scheme has an obvious advantage as all involved reactions proceed in an acidic medium that does not affect the COSS core known to be extremely unstable in the presence of nucleophiles. We found that the coupling efficacy depends on the ligand in view of steric hindrance and electrostatic repulsion. Thus, octapeptide derivatives were eightfold presented on a COSS scaffold, whereas for more bulky ligands lower oligomers were detected. Nevertheless, for the first time the scaffold-based conjugation of miniproteins comprising a backbone of about thirty amino acids with a structure-defining cystine knot was successfully accomplished without the loss of ligand bioactivity.

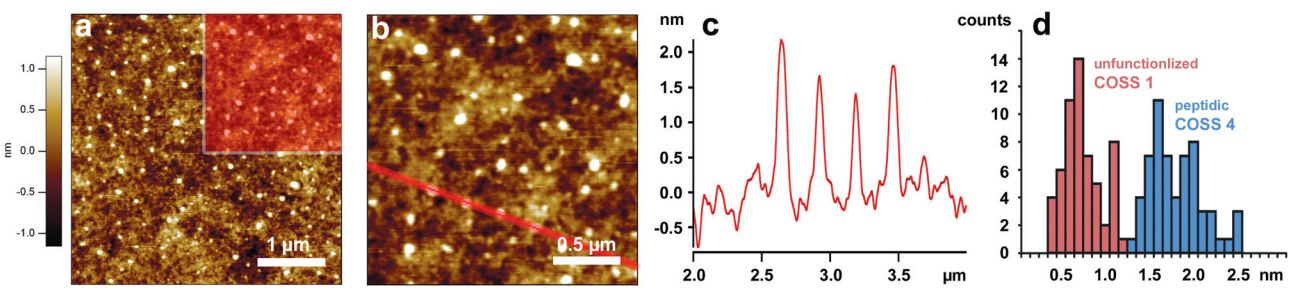

Fig. 3 (a) AFM topography image of a uniformly distributed COSS–peptide particle **3** on a mica surface; (b) image extension displaying the trend of the section line; (c) profile of four adjacent particles; (d) comparative histogram depicting the size distribution of **1** and **4**.

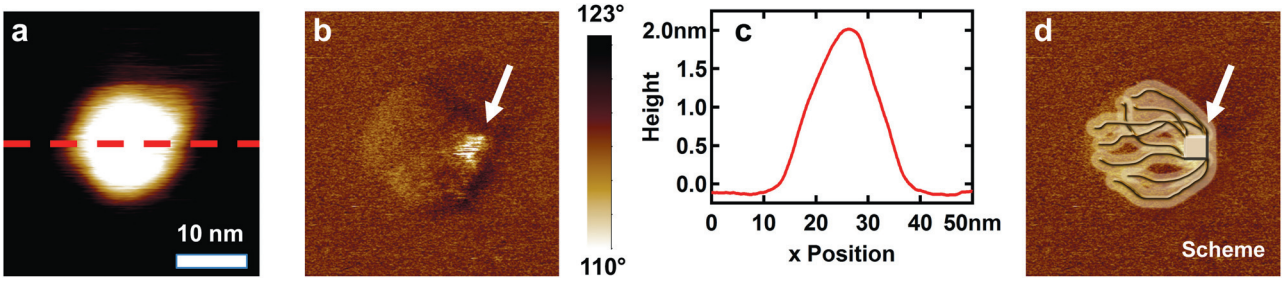

Fig. 4 High-resolution image of a single COSS–peptide particle **4** using bimodal atomic force microscopy. (a) Topography image and (b) profile of a single particle. (c) Corresponding second eigenmode phase image. The image reveals a bright region at the right area of the particle. (d) Schematic structure of the particle deduced from the phase image shown in (b).

AFM experiments conducted in the present study provided further knowledge on the size of COSS allowing us to consider them as picoscaffolds growing upon bioconjugation to nano-dimension.

Detailed studies concerning the bioactivity of COSS-assembled conjugates are currently ongoing, with constructs **6** and **9** being of particular interest. They can provide an interface for the non-covalent oligomerization of proteins fused either to a complementary Ecoil or to calmodulin. Thus, oligomerization can occur *via* the formation of a Kcoil/Ecoil leucine zipper,[48] or through tight binding to mastoparan,[46] respectively.

Experimental

Peptide synthesis

Microwave-assisted Fmoc-SPPS of peptide ligands was performed on a CEM *liberty*® peptide synthesizer equipped with a CEM *discover*® SPS microwave (CEM GmbH). As solid supports 2-CT-resin-Gly-OH from Iris Biotech GmbH (**p4** and **p5**), AmphiSphere™ 40 RAM resin from Varian Inc. (**p6**, **p7** and **p8**) and NovaSyn®TGR resin from Merck KGaA (**p8**) were used. After cleavage, cysteine-free crude products were oxidized using 10 equiv. of sodium periodate in PBS buffer for 10 min. The reaction product was isolated by RP-HPLC using a Varian 940-LC equipped with a YMC Europe GmbH C18 column (250 × 20 mm; S- 4 µm, 8 nm). Oxidative folding[59] of hexathiol precursors was followed by RP-HPLC purification. The resulting cystine knots were submitted to the above-described periodate oxidation procedure.

Synthesis of octa(aminopropyl) COSS 1

The synthesis of **1** was performed according to the reported procedure.[10]

Synthesis of scaffold 2

10 mg (1 equiv., 0.009 mmol) of **1**, 90 mg (5 equiv. per ammonium group, 0.35 mmol) of Eei protected and NHS activated aminooxyacetic acid[40] and 240 µL (20 equiv. per ammonium group, 178.1 mg, 1.38 mmol) of dry DIEA were dissolved in 3 mL of dry DMF. After 12 hours of stirring, full conversion of **1** into **2** was confirmed by LC-MS monitoring. Subsequently, the solvent and base were removed *in vacuo*. The resulting crude product was purified *via* RP-HPLC using a semi-preparative C4 column (300 × 20 mm, 5 µ, PSS Polymer Standards Service GmbH) and a linear gradient of 90% aq. MeCN (10 → 100% B in 63 min) preceded by 10 min isocratic 10% B at a flow rate of 10 mL min^{-1} with t_R = 48.0 min. Yield after RP-HPLC purification: 5.7 mg (33%).

HR-MS: calc. for $C_{72}H_{136}N_{16}O_{36}Si_8$ (+2): 1013.3801, meas. 1013.3800 $[M + 2H]^{2+}$, 1024.3710 $[M + H + Na]^{2+}$, 1035.3622 $[M + 2Na]^{2+}$; ATR-IR: ν 702 w, 1114 vs, 1308 m, 1378 w, 1540 w, 1651 m, 2933 vw, 3332 vw cm^{-1}, ^{29}Si NMR IGATED (99 MHz, $CDCl_3$): δ −66.85.

Synthesis of scaffold 3

50 mg (1 equiv., 0.043 mmol) of **1**, 347 mg Boc-aminooxy acetic acid (5.3 equiv. per ammonium group, 1.815 mmol), 674 mg HATU (5.2 equiv. per ammonium group, 1.773 mmol) and 112.5 µL dry collidine (120.8 mg, 2.9 equiv. per ammonium group, 0.997 mmol) were dissolved in 8 mL dry MeCN. After 12 hours of stirring full conversion of **1** into **3** was confirmed *via* LC-MS monitoring. Subsequently, the solvent and base were removed *in vacuo*. The resulting crude product was purified *via* RP-HPLC using a semi-preparative C8 column (250 × 20 mm, 5 µ, Phenomenex Inc.) and a linear gradient of 90% aq. MeCN in 0.1% aq. TFA (40 → 100% B in 20 min) preceded by 5 min isocratic 40% B at a flow rate of 18 mL min^{-1} with t_R = 16.5 min. Yield after RP-HPLC purification: 3.6 mg (4%).

HR-MS: calc. for $C_{80}H_{154}N_{16}O_{44}Si_8$ (+2): 1133.4224, meas. 1133.4216 $[M + 2H]^{2+}$; ATR-IR: ν 1115 vs, 1286 m, 1371 w, 1567 w, 1661 m, 1729 m, 2944 vw, 2989 vw, 3327 vw, ^{29}Si NMR (99 MHz, $CDCl_3$): δ −66.90.

Conjugation of peptidic ligands on aminooxy COSS 3

0.1 mg (1 equiv., 0.041 µmol) of **3** were dissolved in 500 µL 50% aq. TFA and 9 equiv. (0.39 µmol) of a corresponding peptidic ligand were added. The reaction process was monitored for 12 hours by LC-MS. The conjugates were isolated *via* RP-HPLC using an analytical C4 column (50 × 1 mm, 5 µ, Phenomenex Inc.) and a linear gradient of MeCN in 0.1% aq. formic acid (2 → 100% in 10 min) at a flow rate of 0.2 mL min^{-1}.

HR-MS: calc. for **4** $C_{424}H_{689}N_{144}O_{140}Si_8$ (+9): 1140.4375, meas. 1140.4393 $[M + 9H]^{9+}$ (see Fig. S9 and S10†), calc. for **5**

$C_{448}H_{705}N_{112}O_{124}Si_8$ (+9): 1096.0051, meas. 1096.0042 $[M + 9H]^{9+}$ (see ESI Fig. S14 and S15†), calc. for **6** $C_{472}H_{862}N_{130}O_{124}Si_8$: 10 565.34, meas. 10 565.37 (see ESI Fig. S17 and S18†), calc. for **7** $C_{418}H_{697}N_{145}O_{139}S_{18}Si_8$: 10 773.51, meas. 10 773.61 (see ESI Fig. S20 and S21†), calc. for **8** $C_{308}H_{496}N_{104}O_{106}S_{12}Si_8$: 7957.15, meas. 7957.22 (see ESI Fig. S23 and S24†), calc. for **9** $C_{384}H_{700}N_{108}O_{130}Si_8$: 9132.97, meas. 9132.98 (see ESI Fig. S26 and S27†).

Yields based on the integration of HPLC traces at 220 nm: 90% (conjugate **4**) and 99% (conjugate **5**).

See the ESI† for full LC-MS and HR-MS data.

Trypsin inhibition assay

The trypsin inhibition assay of **7** was performed according to the reported procedure.[56]

High resolution imaging of COSS–peptide particles using bimodal atomic force microscopy

Tapping mode atomic force microscopy measurements were performed on COSS–peptide particles randomly distributed on a mica surface. The resonance frequency of the cantilever (PPP-ZEIHR and PPP-NCH from NanoandMore GmbH, Wetzlar, Germany) was f_1 = 120–320 kHz and a free amplitude of $A_{01} \approx 10$ nm was chosen. We paid careful attention to operate the AFM in the net attractive regime where van der Waals forces dominate the tip–sample interaction by keeping the free amplitude low and using a relatively high setpoint amplitude $A_1/A_{01} \approx 0.9$. This operation regime is comparably gentle to the sample surface avoiding excessive indentation of the tip apex into the surface structure.

High-resolution images on single COSS–peptide particles were accomplished using bimodal atomic force microscopy.[60–66] Compared to the conventional tapping mode, the cantilever was excited simultaneously at the first two flexural eigenmodes. The amplitude of the first eigenmode was kept constant varying the distance between a tip and a sample (as in conventional tapping). Additionally, the amplitude and phase shift of the second eigenmode sensed compositional variations of the sample with very high accuracy. The cantilevers' resonance frequencies (PPP-ZEIHR Cantilever) were as follows: f_1 = 127 kHz and f_2 = 781 kHz for the first and second oscillations, respectively. The free amplitude of the oscillating cantilever was excited to A_{01} = 5 nm and A_{02} = 0.5–1 nm.

AFM image processing

All topography images were 1st order flattened in order to remove image tilt. A Gauss filter was applied to enhance the signal-to-noise ratio.

Acknowledgements

We acknowledge the collaboration with Prof. Dr Robert Stark (Center of Smart Interfaces, Technische Universität Darmstadt) with respect to AFM measurements in the frame of the LOEWE Soft Control consortium. We thank Volker Schmidts (Clemens-Schöpf Institute of Organic Chemistry and Biochemistry, Technische Universität Darmstadt) for the performance of ^{29}Si-NMR experiments on **3**.

References

1 P. H. Ehrlich, *J. Theor. Biol.*, 1979, **81**, 123–127.
2 S. M. Deyev and E. N. Lebedenko, *Bioassays*, 2008, **30**, 904–918.
3 D. Wright and L. Usher, *Curr. Org. Chem.*, 2001, **5**, 1107–1131.
4 R. J. Pieters, *Org. Biomol. Chem.*, 2009, **7**, 2013–2025.
5 S. P. Liu, L. Zhou, R. Lakshminarayanan and R. W. Beuerman, *Int. J. Pept. Res. Ther.*, 2010, **16**, 199–213.
6 J. E. Gestwicki, C. W. Cairo, L. E. Strong, K. A. Oetjen and L. L. Kiessling, *J. Am. Chem. Soc.*, 2002, **124**, 14922–14933.
7 J. F. Brown, L. H. Vogt and P. I. Prescott, *J. Am. Chem. Soc.*, 1964, **86**, 1120–1125.
8 D. B. Cordes, P. D. Lickiss and F. Rataboul, *Chem. Rev.*, 2010, **110**, 2081–2173.
9 H. Mori, Y. Miyamura and T. Endo, *Langmuir*, 2007, **23**, 9014–9023.
10 F. J. Feher and K. D. Wyndham, *Chem. Commun.*, 1998, 323–324.
11 V. Ervithayasuporn, X. Wang and Y. Kawakami, *Chem. Commun.*, 2009, 5130–5132.
12 S. Fabritz, D. Heyl, V. Bagutski, M. Empting, E. Rikowski, H. Frauendorf, I. Balog, W.-D. Fessner, J. J. Schneider, O. Avrutina and H. Kolmar, *Org. Biomol. Chem.*, 2010, **8**, 2212–2218.
13 B. Trastoy, M. Eugenia Perez-Ojeda, R. Sastre and J. Luis Chiara, *Chem.–Eur. J.*, 2010, **16**, 3833–3841.
14 U. Dittmar, B. J. Hendan, U. Flörke and H. C. Marsmann, *J. Organomet. Chem.*, 1995, **489**, 185–194.
15 B. W. Manson, J. J. Morrison, P. I. Coupar, P. A. Jaffres and R. E. Morris, *J. Chem. Soc., Dalton Trans.*, 2001, 1123–1127.
16 R. Tamaki, Y. Tanaka, M. Z. Asuncion, J. W. Choi and R. M. Laine, *J. Am. Chem. Soc.*, 2001, **123**, 12416–12417.
17 T. L. Kaneshiro, X. Wang and Z.-R. Lu, *Mol. Pharm.*, 2007, **4**, 759–768.
18 K. Tanaka, K. Inafuku, K. Nakab and Y. Chujo, *Org. Biomol. Chem.*, 2008, **6**, 3899–3901.
19 F. J. Feher, K. D. Wyndham, M. A. Scialdone and Y. Hamuro, *Chem. Commun.*, 1998, 1469–1470.
20 D. Heyl, E. Rikowski, R. C. Hoffmann, J. J. Schneider and W.-D. Fessner, *Chem.–Eur. J.*, 2010, **16**, 5544–5548.
21 J. Henig, E. Toth, J. Engelmann, S. Gottschalk and H. A. Mayer, *Inorg. Chem.*, 2010, **49**, 6124–6138.
22 Y.-C. Lin and S.-W. Kuo, *Polym. Chem.*, 2012, **3**, 162–171.
23 S.-W. Kuo, H.-F. Lee, W.-J. Huang, K.-U. Jeong and F.-C. Chang, *Macromolecules*, 2009, **42**, 1619–1626.
24 V. V. Rostovtsev, L. G. Green, V. V. Fokin and K. B. Sharpless, *Angew. Chem., Int. Ed.*, 2002, **41**, 2596–2599.
25 O. Avrutina, M. Empting, S. Fabritz, M. Daneschdar, H. Frauendorf, U. Diederichsen and H. Kolmar, *Org. Biomol. Chem.*, 2009, **7**, 4177–4185.
26 E. Rikowski and H. C. Marsmann, *Polyhedron*, 1997, **16**, 3357–3361.
27 S.-W. Kuo and H.-T. Tsai, *Polymer*, 2010, **51**, 5695–5704.
28 Y.-C. Lin and S.-W. Kuo, *J. Polym. Sci., Part A: Polym. Chem.*, 2011, **49**, 2127–2137.
29 H. Sigel and R. B. Martin, *Chem. Rev.*, 1982, **82**, 385–426.
30 A. Jancso, K. Andras, B. Gyurcsik, N. V. Nagy and T. Gajda, *J. Inorg. Biochem.*, 2009, **103**, 1634–1643.
31 M. Lo Conte, S. Staderini, A. Chambery, N. Berthet, P. Dumy, O. Renaudet, A. Marra and A. Dondoni, *Org. Biomol. Chem.*, 2012, **10**, 3269–3277.
32 A. Dondoni, A. Massi, P. Nanni and A. Roda, *Chem.–Eur. J.*, 2009, **15**, 11444–11449.
33 A. Dirksen, T. M. Hackeng and P. E. Dawson, *Angew. Chem., Int. Ed.*, 2006, **45**, 7581–7584.
34 O. Renaudet, D. Boturyn and P. Dumy, *Bioorg. Med. Chem. Lett.*, 2009, **19**, 3880–3883.
35 K. F. Geoghegan and J. G. Stroh, *Bioconjugate Chem.*, 1992, **3**, 138–146.
36 J. C. Spetzler and T. Hoeg-Jensen, *Tetrahedron Lett.*, 2002, **43**, 2303–2306.
37 T. Groth and M. Meldal, *J. Comb. Chem.*, 2001, **3**, 34–44.
38 I. P. Decostaire, D. Lelievre, H. Zhang and A. F. Delmas, *Tetrahedron Lett.*, 2006, **47**, 7057–7060.

39 S. Foillard, M. O. Rasmussen, J. Razkin, D. Boturyn and P. Dumy, *J. Org. Chem.*, 2008, **73**, 983–991.
40 V. Dulery, O. Renaudet and P. Dumy, *Tetrahedron*, 2007, **63**, 11952–11958.
41 R. O. Hynes, *Cell*, 1992, **69**, 11–25.
42 R. H. Kimura, A. M. Levin, F. V. Cochran and J. R. Cochran, *Proteins*, 2009, **77**, 359–369.
43 R. Fontana, M. A. Mendes, B. M. de Souza, K. Konno, L. M. M. Cesar, O. Malaspina and M. S. Palma, *Peptides*, 2004, **25**, 919–928.
44 A. Romanelli, L. Moggio, R. C. Montella, P. Campiglia, M. Iannaccone, F. Capuano, C. Pedone and R. Capparelli, *J. Pept. Sci.*, 2011, **17**, 348–352.
45 A. R. Means and J. R. Dedman, *Nature*, 1980, **285**, 73–77.
46 D. A. Malencik and S. R. Anderson, *Biochem. Biophys. Res. Commun.*, 1983, **114**, 50–56.
47 O. Avrutina, H. U. Schmoldt, D. Gabrijelcic-Geiger, D. Le Nguyen, C. P. Sommerhoff, U. Diederichsen and H. Kolmar, *Biol. Chem.*, 2005, **386**, 1301–1306.
48 B. Tripet, L. Yu, D. L. Bautista, W. Y. Wong, R. T. Irvin and R. S. Hodges, *Protein Eng.*, 1996, **9**, 1029–1042.
49 B. Steinmann, A. Christmann, T. Heiseler, J. Fritz and H. Kolmar, *Appl. Environ. Microbiol.*, 2010, **76**, 5563–5569.
50 B. Apostolovic, M. Danial and H.-A. Klok, *Chem. Soc. Rev.*, 2010, **39**, 3541–3575.
51 C. P. Sommerhoff, O. Avrutina, H.-U. Schmoldt, D. Gabrijelcic-Geiger, U. Diederichsen and H. Kolmar, *J. Mol. Biol.*, 2010, **395**, 167–175.
52 A. Heitz, O. Avrutina, D. Le-Nguyen, U. Diederichsen, J.-F. Hernandez, J. Gracy, H. Kolmar and L. Chiche, *BMC Struct. Biol.*, 2008, 8.
53 I. Coin, M. Beyermann and M. Bienert, *Nat. Protocols*, 2007, **2**, 3247–3256.
54 L. Moroder, D. Besse, H. J. Musiol, S. RudolphBohner and F. Siedler, *Biopolymers*, 1996, **40**, 207–234.
55 S. Krause, H.-U. Schmoldt, A. Wentzel, M. Ballmaier, K. Friedrich and H. Kolmar, *FEBS J.*, 2007, **274**, 86–95.
56 M. Empting, O. Avrutina, R. Meusinger, S. Fabritz, M. Reinwarth, M. Biesalski, S. Voigt, G. Buntkowsky and H. Kolmar, *Angew. Chem., Int. Ed.*, 2011, **50**, 5207–5211.
57 J. N. Israelachvili, *Intermolecular and Surface Forces*, Elsevier Inc., 2011.
58 A. Knoll, R. Magerle and G. Krausch, *Macromolecules*, 2001, **34**, 4159–4165.
59 O. Avrutina, H. U. Schmoldt, H. Kolmar and U. Diederichsen, *Eur. J. Org. Chem.*, 2004, 4931–4935.
60 T. R. Rodriguez and R. Garcia, *Appl. Phys. Lett.*, 2004, **84**, 449–451.
61 S. Patil, N. F. Martinez, J. R. Lozano and R. Garcia, *J. Mol. Recognit.*, 2007, **20**, 516–523.
62 R. W. Stark, N. Naujoks and A. Stemmer, *Nanotechnology*, 2007, **18**, 065502.
63 N. F. Martinez, J. R. Lozano, E. T. Herruzo, F. Garcia, C. Richter, T. Sulzbach and R. Garcia, *Nanotechnology*, 2008, **19**, 163118.
64 C. Dietz, M. Zerson, C. Riesch, A. M. Gigler, R. W. Stark, N. Rehse and R. Magerle, *Appl. Phys. Lett.*, 2008, **92**, 143107.
65 J. W. Li, J. P. Cleveland and R. Proksch, *Appl. Phys. Lett.*, 2009, **94**, 163118.
66 C. Dietz, E. T. Herruzo, J. R. Lozano and R. Garcia, *Nanotechnology*, 2011, **22**, 125708.